Journal of Orthopaedic Translation 46 (2024) 103–115

Contents lists available at ScienceDirect

Journal of Orthopaedic Translation

journal homepage: www.journals.elsevier.com/journal-of-orthopaedic-translation

Exosomes from umbilical cord mesenchymal stem cells ameliorate intervertebral disc degeneration via repairing mitochondrial dysfunction

Shu Jia [a,b], Tao Yang [c], Sheng Gao [c], Luyue Bai [c], Zhiguo Zhu [a,b], Siqi Zhao [c], Yexin Wang [c], Xiao Liang [c], Yanpeng Li [c], Longfei Gao [c], Zifang Zhang [c], Xu Gao [d], Dongru Li [e], Shang Chen [a], Bin Zhang [f], Chunyang Meng [a,c,*]

[a] *Clinical Research Team of Spine & Spinal Cord Diseases, Medical Research Center, Affiliated Hospital of Jining Medical University, 89 Guhuai Road, Jining, Shandong Province, 272000, China*
[b] *Postdoctoral Mobile Station, Shandong University of Traditional Chinese Medicine, 4655 Daxue Road, Jinan, Shandong Province, 250355, China*
[c] *Department of Spine Surgery, Affiliated Hospital of Jining Medical University, 89 Guhuai Road, Jining, Shandong Province, 272000, China*
[d] *Department of Medicine, Qingdao University, 38 Dengzhou Road, Qingdao, Shandong Province, 266021, China*
[e] *Department of Clinical Medical College, Jining Medical University, 45 Jianshe Road, Jining, Shandong Province, 272000, China*
[f] *Department of Laboratory Medicine, Affiliated Hospital of Jining Medical University, 89 Guhuai Road, Jining, Shandong Province, 272000, China*

ARTICLE INFO

Keywords:
Umbilical cord mesenchymal stem cells
Exosomes
Mitochondrion
Intervertebral disc degeneration

ABSTRACT

Background: Reactive oxygen species (ROS), predominantly generated by mitochondria, play a crucial role in the pathogenesis of intervertebral disc degeneration (IVDD). Reduction of ROS levels may be an effective strategy to delay IVDD. In this study, we assessed whether umbilical cord mesenchymal stem cell-exosomes (UCMSC-exos) can be used to treat IVDD by suppressing ROS production caused by mitochondrial dysfunction.

Materials and methods: Human UCMSC-exos were isolated and identified. Nucleus pulposus cells (NPCs) were stimulated with H_2O_2 in the presence or absence of exosomes. Then, 4D label free quantitative (4D-LFQ) proteomics were used to analyze the differentially expressed (DE) proteins. Mitochondrial membrane potential (MMP), mitochondrial ROS and protein levels were determined via immunofluorescence staining, flow cytometry and western blotting respectively. Additionally, high-throughput sequencing was performed to identify the DE miRNAs in NPCs. Finally, therapeutic effects of UCMSC-exos were investigated in a puncture-induced IVDD rat model. Degenerative grades of rat IVDs were assessed using magnetic resonance imaging and histochemical staining.

Results: UCMSC-exos effectively improved the viability of NPCs and restored the expression of the extracellular matrix (ECM) proteins, collagen type II alpha-1 (COL2A1) and matrix metalloproteinase-13 induced by H_2O_2. Additionally, UCMSC-exos not only reduced the total intracellular ROS and mitochondrial superoxide levels, but also increased MMP in pathological NPCs. 4D-LFQ proteomics and western blotting further revealed that UCMSC-exos up-regulated the levels of the mitochondrial protein, mitochondrial transcription factor A (TFAM), in H_2O_2-induced NPCs. High-throughput sequencing and qRT-PCR uncovered that UCMSC-exos down-regulated the levels of miR-194-5p, a potential negative regulator of TFAM, induced by H_2O_2. Finally, in vivo results showed that UCMSC-exos injection improved the histopathological structure and enhanced the expression levels of COL2A1 and TFAM in the rat IVDD model.

Conclusions: Our findings suggest that UCMSC-exos promote ECM synthesis, relieve mitochondrial oxidative stress, and attenuate mitochondrial dysfunction in vitro and in vivo, thereby effectively treating IVDD.

The translational potential of this article: This study provides solid experimental data support for the therapeutic effects of UCMSC-exos on IVDD, suggesting that UCMSC-exos will be a promising nanotherapy for IVDD.

* Corresponding author. Department of Spine Surgery, Affiliated Hospital of Jining Medical University, 89 Guhuai Road, Jining, Shandong Province, 272000, China.
E-mail address: mengchunyang1600@mail.jnmc.edu.cn (C. Meng).

https://doi.org/10.1016/j.jot.2023.10.004
Received 25 May 2023; Received in revised form 4 October 2023; Accepted 11 October 2023

1. Introduction

Intervertebral disc degeneration (IVDD) is a major cause of disability associated with low back pain and neck pain [1–3]. IVD comprises the central nucleus pulposus (NP), surrounding annulus fibrosus (AF) and upper and lower cartilage endplates (CEP). NP is a hydrated gelatinous tissue consisting of type II collagen, elastin fibers and aggrecan that responds to diverse external mechanical stimuli [4]. NP cells (NPCs) are the primary cell types in NP that are responsible for the synthesis and maintenance of the extracellular matrix (ECM). IVDD is characterized by decreased NPCs proliferation and loss of extracellular matrix [5]. The current clinical therapies for IVDD include conservative approaches, intervertebral disc displacement, spinal fusion and percutaneous endoscopic lumbar discectomy (PELD). However, recurrent disc herniation and adjacent segment diseases might be an inevitable issue arising for both surgeons and patients [6]. Therefore, novel approaches are needed to effectively retain the normal structure of IVD and delay the progression of IVDD.

Mesenchymal stem cells (MSCs) are an ideal cell source for IVD tissue engineering owing to their multipotent differentiation capacity and self-renewal ability. MSCs can differentiate into an NP-like phenotype to reconstruct the IVD structure [7,8]. Furthermore, MSCs possess anti-oxidant and anti-inflammatory properties that protect NPCs from harsh microenvironments [9,10]. However, acidic pH conditions of IVD are unfavorable for the proliferation of MSCs and the short survival time of transplanted MSCs (<1 week) may hinder MSC therapy [11,12]. MSC-secreted exosomes can potentially be used for IVDD treatment [13,14]. Exosomes are vesicles with diameter of 30–100 nm that originate from multivesicular endosomes and are released by cells into the extracellular environment. Compared with MSCs, exosomes have obvious advantages, such as more stable properties, low immunogenicity and avoidance of MSCs aging [15,16]. Various bioactive molecules, including proteins, lipids, mRNAs and non-coding RNAs are transported via exosomes into recipient cells. MSC-exos deliver microRNAs (miRNAs), such as miR-105-5p, miR-21 and miR-26, to degenerated NPCs and thereby improve IVDD [17–19]. Moreover, MSC-exos replenish anti-oxidant proteins, including peroxiredoxin-1 and glutathione peroxidase 4, to protect NPCs from oxidative stress [20].

Pathomechanism of IVDD is closely associated with excessive reactive oxygen species (ROS) generation and oxidative stress [21]. Accumulation of cellular and mitochondrial ROS is observed in degenerated NPCs [22]. Mitochondrial dysfunction is the main cause of excessive ROS production, which damages mitochondria and causes NPC apoptosis and pyroptosis, ultimately leading to IVDD [23,24]. PINK1/Parkin-mediated mitophagy effectively degrades the damaged mitochondria and restores the mitochondrial homeostasis. However, excessive mitophagy causes elimination of mitochondria, leading to apoptosis [25,26]. The maintenance of mitophagy at a normal level is beneficial for protecting NPCs against oxidative stress and alleviating IVDD [27,28]. Accumulating evidence suggests that exosomes are also involved in intercellular mitochondrial communication. BMSC-exos can replenish mitochondrial DNA and proteins to restore the normal mitochondrial function in degenerated NPCs [20]. However, no studies have focused on the modulation of mitochondrial function by exosomes originating from umbilical cord–derived MSCs (UCMSC-exos) during IVDD.

In this study, we isolated UCMSC-exos and investigated their therapeutic effects on degenerated human NPCs and rat IVDD model. We found that UCMSC-exos not only promoted the proliferation of NPCs, but also restored the ECM composition. Additionally, UCMSC-exos repaired the damaged mitochondria by increasing the expression of mitochondrial protein, mitochondrial transcription factor A (TFAM), in H_2O_2-induced NPCs to suppress ROS production. Further research showed that UCMSC-exos down-regulated the levels of miR-194-5p, a potential negative regulator of TFAM, induced by H_2O_2. Finally, in vivo experiments revealed that UCMSC-exos significantly delayed the progression of degeneration in a rat model of IVDD.

2. Materials and methods

2.1. Isolation of human degenerative NPCs

Degenerative NP samples were collected from six patients with IVDD who underwent surgery at the Affiliated Hospital of Jining Medical University. Detailed information of NPC donors is shown in Table 1. NP tissues were cut into 1 mm^3 fragments and digested with 0.2% type II collagenase (Solarbio, Beijing, China) for 2–3 h at 37°C. Tissue debris was removed by passing through a 200 mesh filter, and the suspension was centrifuged at 1000 rpm for 5 min. The cell pellet was resuspended in Dulbecco's modified Eagle's medium (DMEM; Gibco, Grand Island, NY, USA) containing 10% fetal bovine serum (FBS; Gibco) and 100 U/mL penicillin-streptomycin (P–S; Gibco) and cultured in a 5% CO_2, 37°C cell incubator. NPCs adhered after 7–10 d and grew to confluence after 3–4 weeks. All procedures were approved by the Ethics Committee of the Affiliated Hospital of Jining Medical University (Ethical approval number: 2021C159). Written informed consent was obtained from all patients prior to the study.

2.2. Isolation of human UCMSCs

Human UCs were obtained from healthy pregnancies in Affiliated Hospital of Jining Medical University. UC tissues were washed in 0.9% normal saline and dissected to remove the blood vessels. The tissues were then cut into 1 mm^3 pieces and placed in plates with DMEM containing 10% FBS and 100 U/mL P–S. Adherent fibroblast-like cells expanded from the tissue pieces after 7–12 d of incubation and proliferated to confluence after 2–3 weeks. All procedures were approved by the Ethics Committee of the Affiliated Hospital of Jining Medical University (Ethical approval number: 2021C159). Written informed consent was obtained from all patients.

2.3. Identification of UCMSC surface antigen phenotypes

UCMSCs were digested with 0.25% EDTA–trypsin and stained with fluorescein isothiocyanate (FITC)-conjugated antibodies for 15 min in the dark at room temperature (RT). MSCs were then washed twice with phosphate-buffered saline (PBS) and resuspended in 200 μL PBS for flow cytometry analysis (Beckman Coulter, CA, USA). The antibodies used were against human antigens CD34, CD45, CD73, CD90, CD105, and HLA-DR (BioLegend, CA, USA). Positive cells were counted and compared to the signal of unstained negative controls.

2.4. Isolation of UCMSC-exos

When the density of UCMSCs reached 50–60%, they were washed with PBS and cultured in DMEM containing exosome-free FBS at 37°C, 5% CO_2. The culture medium was collected and centrifuged at 300×*g* for 15 min at 4°C and subsequently at 2000×*g* for 15 min to remove dead cells and cellular debris. The supernatant was transferred to an Amicon Ultra-15 Centrifugal Filter Unit (Merck–Millipore, Darmstadt, Germany) and centrifuged at 4000×*g*. The ultrafiltered liquid was slowly laid

Table 1
Information of NPC donors.

Sample	Gender	Age	Herniated disc	Pfirrmann grading
NP1	Male	35	L5/S1	III
NP2	Male	26	L5/S1	II
NP3	Female	41	L5/S1	IV
NP4	Female	31	L5/S1	III
NP5	Male	31	L5/S1	III
NP6	Male	14	L5/S1	II

above the 30% sucrose/deuterium oxide solution in a Ultra-Clear™ tube (Beckman Coulter, Brea, CA, USA) and ultracentrifuged at 100,000×g, 4°C for 1 h. The exosome pellets were ultrafiltered twice with PBS to remove residual sucrose/deuterium oxide. Ultimately, exosomes were resuspended in PBS and filtered using a 0.22-μm sterile filter (Merck–Millipore).

2.5. Characterization of UCMSC-exos

The exosome solution was added to a Formvar-carbon-loaded copper grid and dried for 20 min. The copper grid was fixed with 1% glutaraldehyde for 5 min, incubated with uranyl oxalate for 5 min and methylcellulose for 10 min on ice. Finally, the copper grid was examined using the transmission electron microscopy (TEM) (H-7650, Hitachi, Tokyo, Japan) at 80 kV to observe the morphology of exosomes. The size distribution and concentration of exosomes were measured using a ZetaView Nanoparticle tracking system (PMX 110, Particle-Metrix, Meerbusch, Germany), and the data was analyzed using ZetaView 8.02.28. Furthermore, the exosomal marker proteins Alix, CD63 and Tsg101 were detected by western blotting.

2.6. Internalization of UCMSC-exos by NPCs

Incubate the exosomes with DiI dye (Thermo Fisher Scientific, Waltham, MA, USA) at 37°C for 30 min and wash twice in PBS by centrifugation. The labelled exosomes were diluted in complete medium and incubated with NPCs at 37°C for 24 h. 4′,6-diamidino-2-phenylindole (DAPI; Thermo Fisher Scientific) was used to stain the nucleus. Stained cells were observed using a laser scanning confocal microscope (Zeiss, Oberkochen, Germany) at the excitation and emission wavelengths of 549 and 565 nm (Ex/Em = 549/565 nm), respectively.

2.7. Western blotting

NPCs were seeded on 6-well plates and cultured overnight. When grown to 80% confluence, cells were treated with 500 μM H_2O_2 for 3 h, followed by incubation with UCMSC-exos (50 μL, 10^{11} particles/mL) for 24 h. Cells were lysed with RIPA buffer for 30 min on ice and centrifuged at 12,000 g, 4°C, 15min. The supernatant was collected and protein concentrations were measured using a BCA protein assay kit. Proteins were separated by SDS-PAGE and transferred to PVDF membranes. The membranes were blocked, incubated with primary antibodies overnight at 4°C and HRP-labelled secondary antibodies for 1 h at RT. Finally, the membranes were exposed to hypersensitive ECL reagent and imaged using a chemiluminescence detector (Tanon Science and Technology Co., Ltd.). ImageJ v.1.46r software (National Institutes of Health) was used to quantify the relative protein expression with β-actin as the control. The primary antibodies used are as follows: Alix (CST, cat no: 92880), CD63 (ABclonal, cat no: A19023), Tsg101 (ABclonal, cat no: A5789), GAPDH (ABclonal, cat no: AC002), COL2A1 (Proteintech, cat no: 28459-1-AP), MMP13 (Abcam, cat no: ab39012), LC3A/B (CST, cat no: D3U4C), PINK1 (CST, cat no: 6946), Actin (ABclonal, cat no: AC026), TFAM (CST, cat no: 8076).

2.8. Immunofluorescence staining

NPCs were seeded on 24-well plates and incubated with UCMSC-exos (12.5 μL, 10^{11} particles/mL, 24 h) with or without pretreatment of H_2O_2 (500 μM, 3 h). Cells were fixed with 4% paraformaldehyde for 10 min, then permeabilized and blocked using 10% FBS containing 0.1% TritonX-100 for 20 min at RT. After washing with PBS, cells were incubated with the primary antibodies at 4°C overnight and 488/543-conjugated secondary antibody for 1 h at RT. Finally, cells were washed with PBS and inverted on glass slides using anti-fluorescence quenching mounting medium with DAPI. The glass slides were imaged using a confocal microscope (Zeiss LSM800; Zeiss AG; magnification, ×630). Relative fluorescence was quantified using ImageJ v.1.46r software (National Institutes of Health). The primary antibodies were against: COL2A1, MMP13 and Ki67 (Proteintech, cat no: 27309-1-AP).

2.9. Assessment of intracellular ROS levels

NPCs were seeded on 6/24-well plates and treated as described above. Cells were incubated with DCFH-DA (10 μM) for 30 min at 37°C in the dark, then washed with serum-free medium to remove excess DCFH-DA. Stained cells were observed by fluorescence microscope and quantified by flow cytometry at Ex/Em = 488/525 nm.

2.10. Measurement of mitochondrial ROS levels

MitoSox Red Mitochondrial Superoxide Indicator (5 μM, 10 min, 37°C) was used to determine mitochondrial ROS production. Stained cells were imaged by fluorescence microscope and quantified by flow cytometry at Ex/Em = 510/580 nm. The MitoBright LT Deep Red (0.1 μM) was incubated with NPCs for 30 min at 37°C to monitor mitochondrial morphology. Stained mitochondria were imaged by confocal microscope at Ex/Em = 640/670 nm.

2.11. Detection of mitochondrial membrane potential (MMP)

MMP was evaluated by measuring JC-1 fluorescence intensity with a mitochondrial membrane potential assay kit (ab113850, Abcam). JC-1 fluorescence intensity was observed by confocal microscope at excitation at Ex/Em = 488/530 nm (JC-1 monomers) and 590 nm (JC-1 aggregates). The ratio of red JC-1 aggregates fluorescence intensity/green JC-1 monomers represents MMP.

2.12. Proteomic profiling

2.12.1. Protein extraction

The samples were added with lysis buffer (1% SDC, 1% protease inhibitor), heated at 95°C for 10 min, lysed by sonication, and the protein concentration was determined using a BCA kit.

2.12.2. Trypsin digestion

The protein solution was reduced with 5 mM dithiothreitol (DTT) for 30 min at 56°C and alkylated with 11 mM iodoacetamide (IAA) for 15 min at RT in the dark. TEAB was used to dilute the concentration of urea to less than 2 M. Trypsin was added at a ratio of 1:50 (trypsin:protein, m/m) for the first digestion overnight and 1:100 (trypsin:protein, m/m) for a second 4 h-digestion. Finally, the peptides were desalted by C18 SPE column.

2.12.3. Liquid chromatography-mass spectrometry (LC-MS) analysis

Peptides were dissolved in mobile phase A and separated using NanoElute ultra-high performance liquid phase system (Bruker Daltonics, Karlsruhe, Germany). Mobile phase A was an aqueous solution containing 0.1% formic acid and 2% acetonitrile, whereas mobile phase B was a solution containing 0.1% formic acid and 100% acetonitrile. Liquid phase gradient settings were: 0–72 min, 7–24% B; 72–84 min, 24–32% B; 84–87 min, 32–80% B; 87–90 min, 80% B. Flow rate was maintained at 450 nL/min. The peptides were subjected to Capillary ion source for ionization followed by a timsTOF Pro mass spectrometer. The ion source voltage was set at 1.75 kV. Precursor ions and fragments were analyzed using high-resolution TOF with an MS/MS scan range from 100 to 1700 *m/z*. The timsTOF Pro was operated in Parallel Accumulation Serial Fragmentation (PASEF) mode. Precursor ions with charge states 0 to 5 were selected for fragmentation, and 10 PASEF-MS/MS scans were acquired per cycle. Precursor ions were excluded from reselection for 30 s.

2.12.4. Data analysis

LC-MS data were processed using MaxQuant search engine (v.1.6.15.0). Tandem mass spectra were searched against the human SwissProt database (20422 entries) and concatenated with reverse decoy database. Trypsin/P was specified as cleavage enzyme, and ≤2 missing cleavages were allowed. The mass tolerance for precursor ions was set at 20 and 5 ppm during the first and main searches, respectively, and the mass tolerance for fragment ions was set at 0.02 Da. Carbamidomethylation on Cys was specified as a fixed modification, and acetylation at the protein N-terminus and oxidation on Met were specified as variable modifications. False discovery rate (FDR) was adjusted to < 1%.

2.12.5. Bioinformatic analysis

To determine the biological and functional properties of differentially expressed proteins (DEPs), sequences were mapped based on Gene Ontology (GO) terms (http://geneontology.org/). GO terms matching was performed with Blast2GO software (v4.5 pipeline5). The ontology includes three categories: biological process, cellular component and molecular function. The signaling pathways of differentially expressed proteins were explored using KEGG analysis (https://www.genome.jp/kegg/). Based on the Fisher's test P value obtained from the enrichment analysis, hierarchical clustering was used to cluster related functions in different groups and plotted into a heatmap. The horizontal direction of the heatmap shows the comparison group, and the vertical direction shows the description of related function (GO and KEGG). The colored blocks indicate the degree of enrichment: red represents strong enrichment and blue represents weak enrichment.

2.13. Identification of differentially expressed (DE) miRNAs by high-throughput sequencing

High-throughput sequencing of miRNAs was conducted by Aksomics Inc. (Shanghai, China). The trimmed miRNA sequences longer than 15 nucleotides were aligned with the genome using Bowtie. miRDeep2 was used for predicting new miRNAs and quantifying miRNAs. Based on the normalization of miRNAs by counts per million (CPM), DE miRNAs were calculated and screened using the R software edgeR. DE miRNAs in H vs C and H + E vs H groups were identified as follows: fold change (FC) > 1.5 and $P < 0.05$.

2.14. Quantitative real-time polymerase chain reaction (qRT-PCR)

Total RNA was extracted from NPCs using TRIzol (Ambion, Austin, TX, USA) according to the manufacturer's instructions. RNA concentration and purity were determined using NanoDrop 2000 (Thermo Fisher Scientific, Waltham, MA, USA). miRNAs were reverse transcribed using a reverse transcription Kit (Accurate Biology, Hunan, China). qRT-PCR was performed by using ultra SYBR mixture (CWbio, Jiangsu, China) on Bio-Rad CFX-96 Real-Time System (Bio-Rad, Foster City, CA, USA). U6 was used as reference gene for miRNA. The relative expressions of miR-194-5p were calculated following the 2-ΔΔ CT method. Primer sequences for qRT-PCR are listed in Table 2.

2.15. Construction of a rat IVDD model

Twenty three-month-old male Sprague–Dawley rats were used to establish the IVDD model as previously reported [29]. Five rats remained intact and were used as negative controls. Fifteen rats were placed in the prone position after anesthesia with 2% (w/v) pentobarbital (40 mg/kg). Rat tails were disinfected using iodinated polyvinylpyrrolidone (PVP–I) before surgery. Two IVDs (Co6/7 and Co8/9) were punctured by a 20-gauge needle from the dorsal side. The needle was inserted vertically through the center of IVD to the opposite side, rotated 360° and held for 10 s. PVP-I was used to sterilize the rat tails after surgery. After two weeks, the rats were randomly divided into three groups (sham: non-injection, PBS and UCMSC-exos) with five rats in each group. Ten microlitres of PBS or UCMSC-exos (10^{11} particles/mL) was slowly injected into the punctured discs using a microlitre syringe with 33-gauge needle (Hamilton, Bonaduz, Switzerland). The injection procedure was repeated every two weeks for two months.

Table 2
The primer sequences. Universal Reverse Primer*: the reverse primer is included with the reverse transcription kit, CAT. NO. AG11716 (Accurate Biology, Hunan, China).

Gene	Forward (5′-3′)	Reverse (5′-3′)
miR-194-5p	TGTAACAGCAACTCCATGTGGA	Universal Reverse Primer*
U6	GGAACGATACAGAGAAGATTAGC	TGGAACGCTTCACGAATTTGCG

2.16. Magnetic resonance imaging (MRI) examination

Rats were anesthetized with 2% pentobarbital 8 weeks after surgery. MRI was performed using a 3.0 T MRI system (Bruker Pharmascan, Ettlingen, Germany). Sagittal T2-weighted imaging was performed using the following settings: time of repetition (TR), 3000 ms; time of echo (TE), 70 ms; slice thickness, 1.5 mm. The degree of IDD was assessed according to Pfirrmann grading system.

2.17. Histological analysis

IVDs were fixed in 4% paraformaldehyde and decalcified in EDTA for 4 weeks. The discs were dehydrated, embedded in paraffin and then cut into 5 μm thick sections. The sections were stained with hematoxylin-eosin (H&E), Safranin O and Alcian blue. For immunofluorescence, the sections were blocked with 5% (w/v) BSA and incubated with primary antibodies against COL2A1 and TFAM, followed by incubation with secondary antibodies conjugated with Alexa Fluor 543. Finally, the sections were scanned by a Zeiss laser confocal microscope.

2.18. Statistical analysis

Data are presented as the mean ± standard deviation (SD) of three independent experiments. Statistical data were analyzed using an unpaired Student's *t*-test or one-way analysis of variance (ANOVA) with the GraphPad Prism 8 software. $P < 0.05$ was considered statistically significant difference.

3. Results

3.1. Characterization of UCMSC-exos

Flow cytometric analysis revealed that the adherent cells isolated from the umbilical cord were positive for MSC markers, CD73, CD90 and CD105, but negative for CD34, CD45 and HLA-DR (Fig. 1A). TEM, NTA and western blotting were used to characterize the morphology, diameter, concentration and protein markers of isolated UCMSC-exos. Exosomes were observed as cup-shaped double-layered membrane structures by TEM (Fig. 1B). The concentration of exosomes was 10^{11} particles/mL and the mean diameter was 100 nm, as measured by NTA (Fig. 1C). Western blotting revealed that the exosomes expressed higher levels of protein markers Alix, CD63 and TSG101 and lower levels of GAPDH than cell lysates (Fig. 1D).

3.2. UCMSC-exos promote the proliferation of human degenerated NPCs

Human degenerated NPCs were isolated from patients with IVDD and identified using safranin O and type II collagen immunochemical staining (Supplementary Fig. 1). UCMSC-exos were labeled with the fluorescent dye DiI and then incubated with NPCs for 24 h. As shown in Fig. 2A, UCMSC-exos were distributed throughout the cytoplasm of

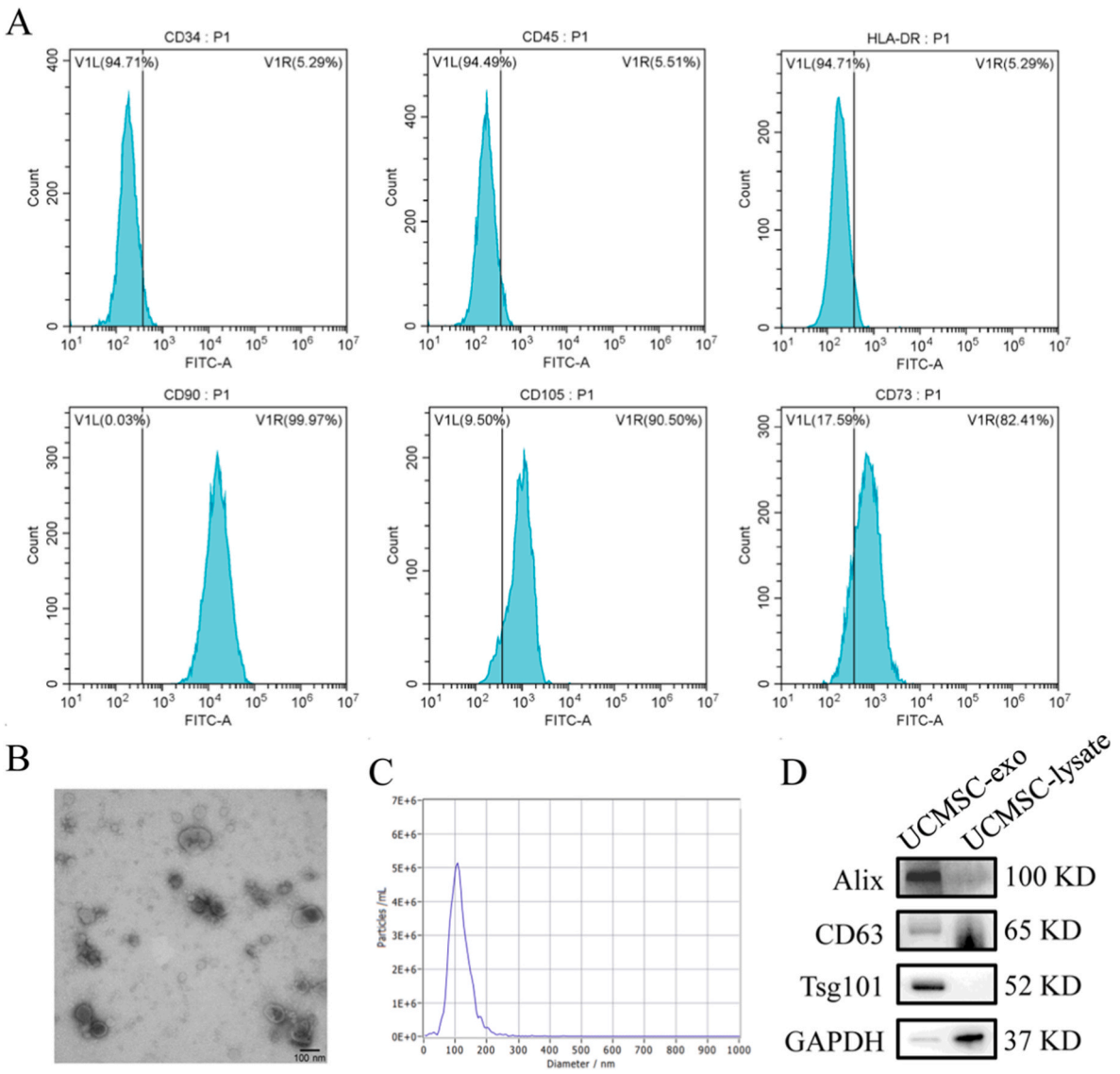

Figure 1. Characterization of UCMSC-exos. (A) Flow cytometry analysis of MSC immunophenotypic profiles including CD90, CD105, CD73 and negative control CD34, CD45, HLA-DR. (B) Representative images of UCMSC-exos by TEM. Scale bar: 100 nm. (C) Particle size distribution of UCMSC-exos measured by NTA. (D) Western blot analysis of exosomal protein markers Alix, CD63, Tsg101 and negative control GAPDH.

NPCs, indicating the internalization of exos by NPCs. Next, we assessed the effect of UCMSC-exos on the proliferative activity of NPCs. As shown in Fig. 2B and C, the proliferative rate of NPCs increased after treatment with UCMSC-exos. Moreover, the Ki67 immunofluorescence assay revealed that UCMSC-exos resulted in a higher proportion of Ki67-positive cells than the control group (Fig. 2D and E). These results suggest that internalized UCMSC-exos promote the proliferation of NPCs.

3.3. UCMSC-exos restore the ECM components of H_2O_2-stimulated NPCs

To explore the protective role of UCMSC-exos on ECM components in H_2O_2-treated NPCs, we assessed the expression of COL2A1 and MMP13. Western blotting revealed that H_2O_2 down-regulated COL2A1 (Fig. 3A and B) and up-regulated MMP13 (Fig. 3E and F) in NPCs, but UCMSC-exos treatment significantly suppressed these effects. Furthermore, immunofluorescence results supported that UCMSC-exos restored COL2A1 expression (Fig. 3C and D) and blocked MMP13 expression (Fig. 3G and H) in NPCs stimulated with H_2O_2. These data indicate that UCMSC-exos can attenuate ECM degeneration in NPCs induced by H_2O_2.

3.4. Proteomic analysis of DEPs between UCMSC-exos-treated and untreated H_2O_2-stimulated NPCs

Using a 4D proteomic approach, we identified the DEPs between UCMSC-exos-treated and untreated H_2O_2-stimulated NPCs. With a threshold of 1.5-fold expression change and $P < 0.05$, we identified 591 DEPs, including 244 up-regulated and 347 down-regulated proteins, in H_2O_2-stimulated NPCs compared to those in the control (unstimulated) group (H vs C). In addition, 335 DEPs were found in the UCMSC-exos-treated group compared with the untreated group after H_2O_2 induction (H_E vs H), of which 121 proteins were up-regulated and 214 proteins were down-regulated (Fig. 4A). Hierarchical clustering of the DEPs between H and C and those between H_E and H was performed based on GO classification. DEPs between the two comparison groups were enriched in ECM organization and mitochondrial respiratory system (Fig. 4B–D). KEGG annotation analysis was used to identify the enriched molecular processes of DEPs in each group. DEPs in the two comparison groups were involved in p53 and calcium signaling pathways, both of which are related to mitochondrial oxidative stress (Fig. 4E). Based on these findings, we demonstrate that UCMSC-exos may alleviate H_2O_2-

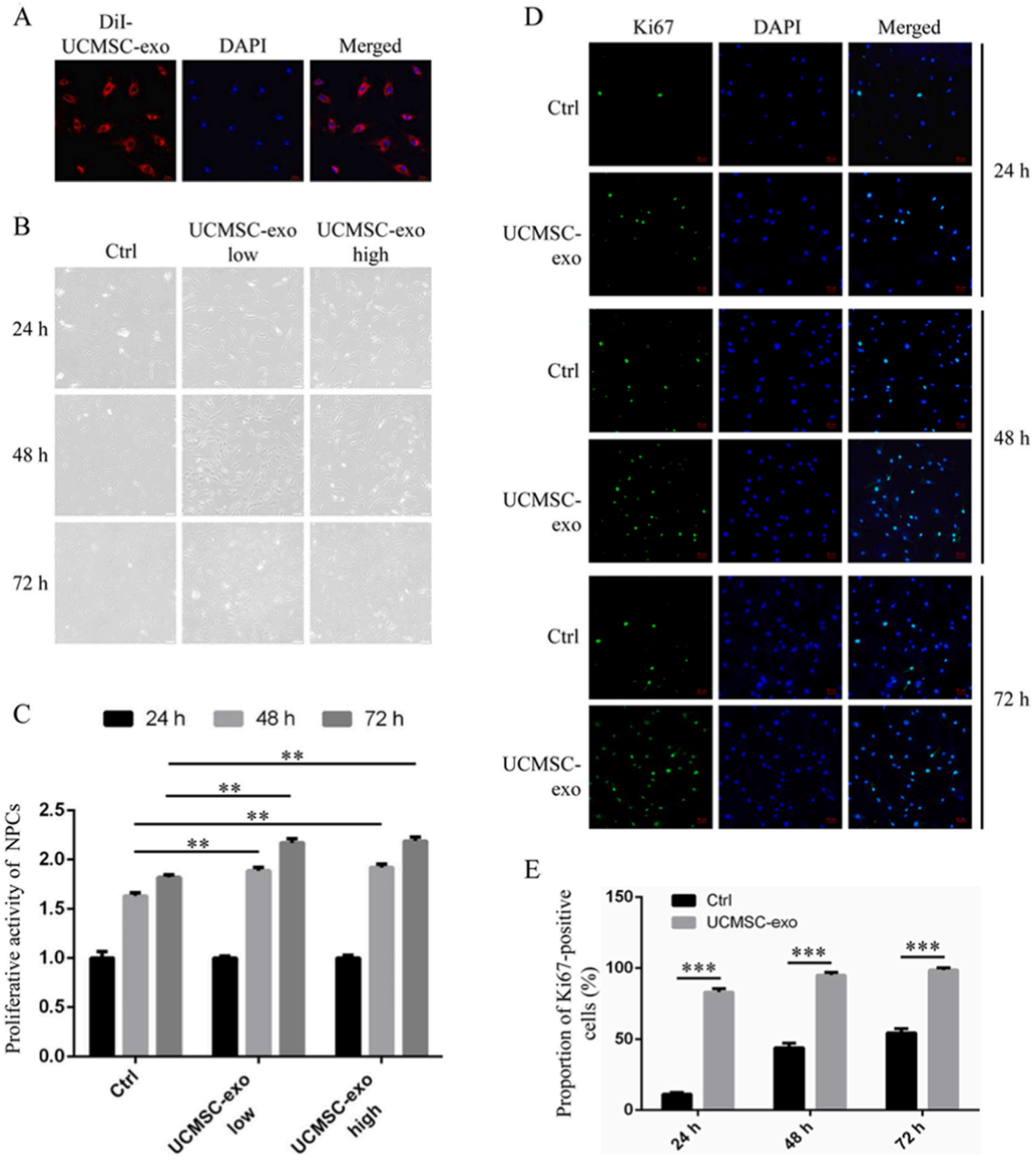

Figure 2. UCMSC-exos promote the proliferation of human degenerated NPCs. (A) The uptake of DiI-labeled UCMSC-exos by NPCs was observed by fluorescence microscopy. Scale bar: 50 μm. (B) Observation of NPC proliferation in response to low (~1.5 × 10^9 particles/mL) and high (~3 × 10^9 particles/mL) concentrations of UCMSC-exos by microscope. (C) The proliferative activity of NPCs was quantified using Image J software. $^{**}P < 0.01$. (D) Immunofluorescence (IF) staining of Ki67 in NPCs after treatment with UCMSC-exos (~3 × 10^9 particles/mL, 24 h). Scale bar: 50 μm. (E) The proportion of Ki67-positive cells was quantified using Image J software. $^{***}P < 0.001$.

induced mitochondrial oxidative stress in NPCs.

3.5. *UCMSC-exos relieve H_2O_2-induced mitochondrial oxidative stress in NPCs*

DCFH-DA was used to measure cellular ROS level in NPCs. Immunofluorescence results showed that the fluorescence intensity of DCFH-DA increased in H_2O_2-stimulated cells versus unstimulated cells, but subsequently decreased after incubation with UCMSC-exos (Fig. 5A and B). Flow cytometric analysis also revealed that H_2O_2 stimulation up-regulated intracellular ROS levels in NPCs, but this effect was suppressed by UCMSC-exos (Fig. 5C and D). Next, mitochondrial superoxide in NPCs was detected using mitoSOX Red which specifically targets the mitochondria. Immunofluorescence results indicated that H_2O_2 up-regulated mitoSOX fluorescence intensity, which was mitigated by UCMSC-exos treatment (Fig. 5E and F). Moreover, flow cytometric analysis was consistent with the fluorescence intensity of mitoSOX (Fig. 5G and H). Taken together, these data reveal that UCMSC-exos treatment reduces ROS production and mitochondrial oxidative stress in H_2O_2-stimulated NPCs.

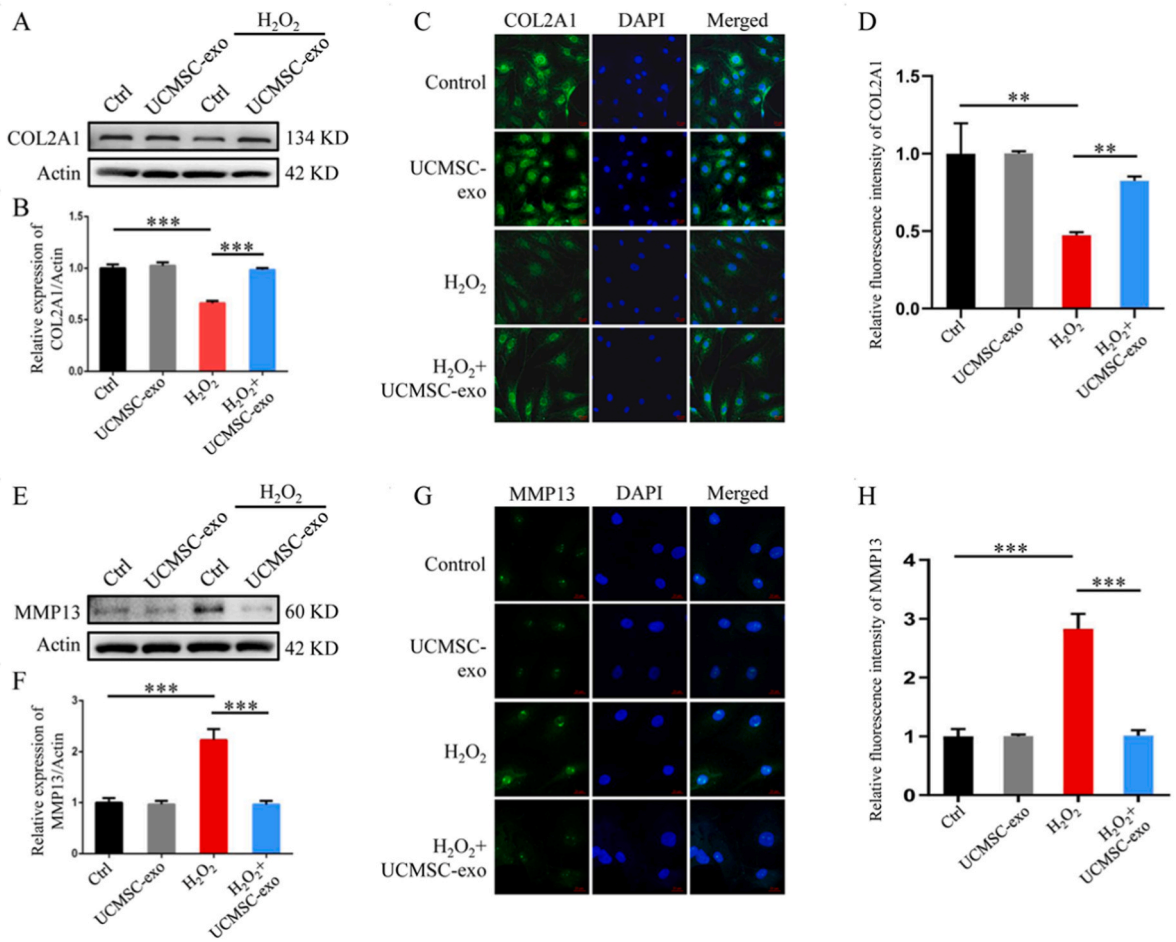

Figure 3. UCMSC-exos restore the ECM components of H_2O_2-stimulated NPCs. (A) Western blot analysis of COL2A1 expression in H_2O_2-stimulated (500 μM, 4 h) NPCs with UCMSC-exos treatment (~3 × 10^9 particles/mL, 24 h). (B) Relative protein expression level of COL2A1 was quantified using Image J software. ***$P <$ 0.001. (C) IF staining of COL2A1 in H_2O_2-stimulated NPCs with UCMSC-exos treatment. Scale bar: 20 μm. (D) Relative fluorescence intensity of COL2A1 was quantified using Image J software. **$P < 0.01$. (E) Measurement of the MMP13 protein level in NPCs by western blot. Cells were exposed to H_2O_2 and treated with UCMSC-exos. (F) Relative protein expression level of MMP13 was quantified using Image J software. ***$P < 0.001$. (G) Representative microscopic images of MMP13 IF staining in NPCs. Scale bar: 20 μm. (H) Relative fluorescence intensity of MMP13 was quantified using Image J software. ***$P < 0.001$.

3.6. UCMSC-exos alleviate mitophagy and mitochondrial dysfunction in H_2O_2-stimulated NPCs

To determine the mitochondrial protective effects of UCMSC-exos, we performed MitoBright Deep Red staining. Compared to the control group, H_2O_2 stimulation resulted in abnormal mitochondria with broken cristae. However, UCMSC-exos attenuated the deterioration of mitochondrial structure (Fig. 6A). JC-1 staining was also performed to assess the effect of UCMSC-exos on the mitochondrial membrane potential (MMP) in H_2O_2-induced cells. Results showed that upon H_2O_2 stimulation the MMP was decreased, but was significantly up-regulated after treatment with UCMSC-exos (Fig. 6B and C). Next, we investigated whether UCMSC-exos affected PINK1/Parkin-mediated mitophagy under H_2O_2 stimulation. Western blot results showed that the expressions of LC3-II and PINK1 were higher in H_2O_2-induced group than the control group. Interestingly, UCMSC-exos suppressed the up-regulation of LC3-II in H_2O_2-stimulated NPCs but augmented the up-regulation of PINK1 (Fig. 6D–G). These data indicate that UCMSC-exos treatment attenuates mitophagy and mitochondrial dysfunction caused by oxidative stress in H_2O_2-induced NPCs.

3.7. UCMSC-exos up-regulate mitochondrial protein TFAM and down-regulate miR-194-5p in H_2O_2-stimulated NPCs

Accumulating evidence suggests that exosomes are also involved in intercellular mitochondrial communication. To explore the mitochondrial proteins affected by UCMSC-exos in NPCs, we intersected the 331 down-regulated proteins in H vs C and 106 up-regulated proteins in H_E vs H using a Venn diagram (Fig. 7A and B). Consequently, 15 proteins including TFAM, DPY30, COX6C, LGR5 and MVK were identified (Fig. 7C). TFAM is essential for maintaining mitochondrial DNA (mtDNA) copy number and transcription initiation. Western blotting revealed that TFAM was significantly down-regulated in NPCs following H_2O_2 stimulation, but up-regulated upon UCMSC-exos treatment (Fig. 7D and E). To explore the mechanism by which UCMSC-exos up-regulate TFAM expression, we performed miRNA sequencing on the three groups (ctrl, H_2O_2, H_2O_2+Exo) and found the differentially expressed miRNAs (Fig. 7F and G). Venn diagram enriched eight miRNAs including miR-194-5p, miR-4508, miR-377-5p, miR-4485-3p, miR-378a-5p, miR-3182, miR-12136 and miR-27b-5p, which were up-regulated in H vs C and down-regulated in H + E vs H (Fig. 7H). Targetscan database predicts that miR-194-5p may negatively regulate TFAM by two interaction sites (Fig. 7I). Consistent with the sequencing data, qRT-PCR results demonstrated that UCMSC-exos down-regulated the expression of miR-194-5p caused by H_2O_2 (Fig. 7J). Furthermore,

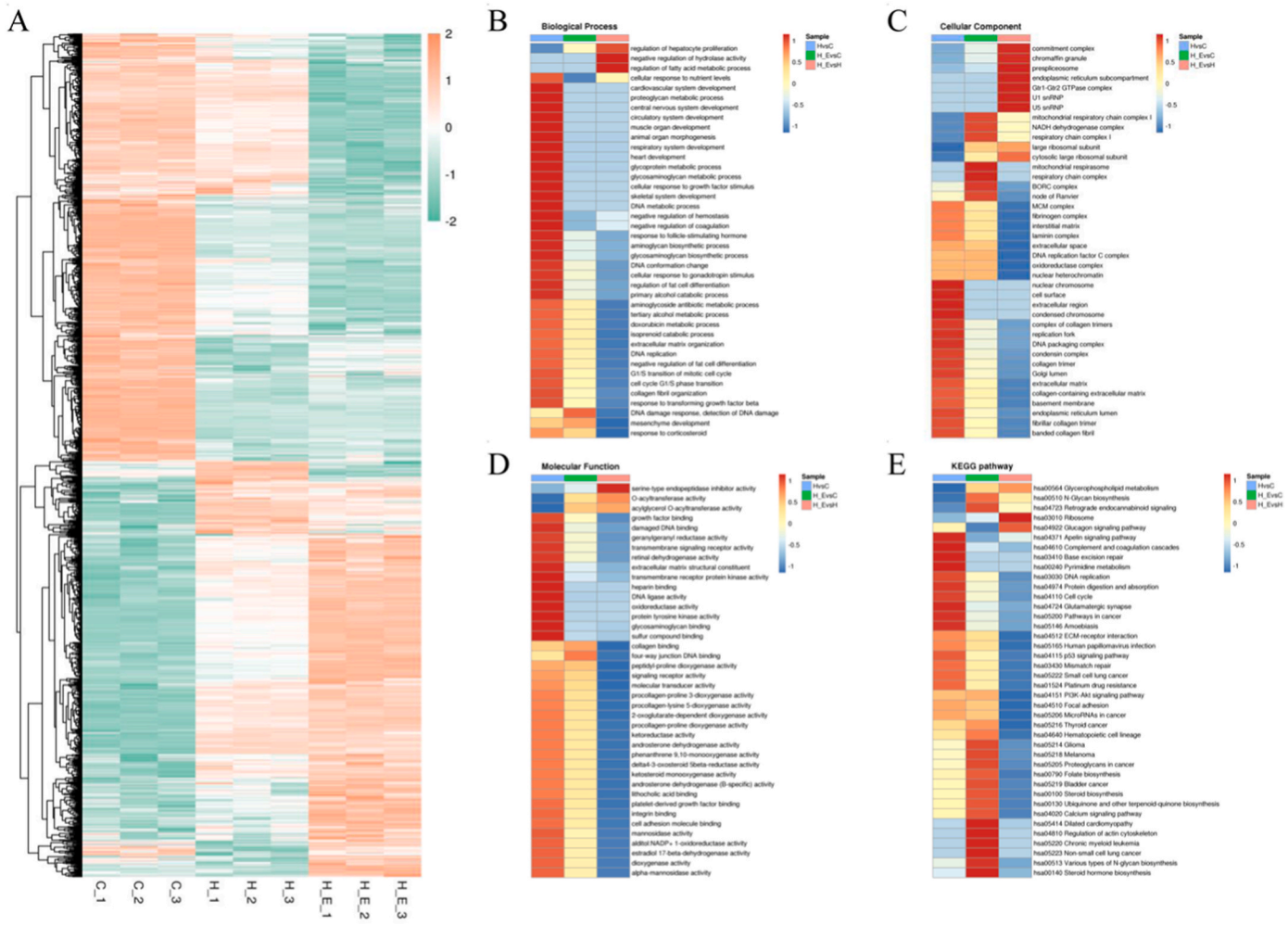

Figure 4. Proteomic analysis of the differentially expressed proteins (DEPs) between UCMSC-exos-treated and untreated H_2O_2-stimulated NPCs. (A) Heatmap of the DEPs in three diverse groups. C: Control group; H: H_2O_2 group; H_E: H_2O_2 + UCMSC-exos group. (B–D) GO enrichment analyses of DEPs in different comparison groups. Relevant functions (BP: biological process, CC: cellular component, MF: molecular function) in different comparison groups were clustered by hierarchical clustering method, and a heatmap was drawn. The horizontal axis shows different comparison groups, and the vertical axis indicates the enriched related functions. Red means strong enrichment, and blue means weak enrichment. All significantly enriched GO terms ($P < 0.05$) involving DEPs are displayed. (E) KEGG pathway enrichment analyses of DEPs. All significantly enriched KEGG pathway terms ($P < 0.05$) involving DEPs are displayed. (For interpretation of the references to color in this figure legend, the reader is referred to the Web version of this article.)

miR-194-5p mimics suppressed TFAM expression, while miR-194-5p inhibitors exert the opposite effect (Fig. 7K and L). These data indicated that UCMSC-exos may up-regulate TFAM expression by inhibiting miR-194-5p in H_2O_2-induced NPCs.

3.8. UCMSC-exos ameliorate IVDD in vivo

To evaluate the role of UCMSC-exos in IVDD progression in vivo, exos were intradiscally injected into a rat model of IVDD. Two independent discs (Co6/7 and Co8/9) per rat were injected with PBS or UCMSC-exos at 2, 4 and 6 weeks after establishment of the IVDD model. The degenerative grades of rat IVDs were assessed by MRI and histochemical staining eight weeks after the induction of IVDD. MRI results suggested that the signal intensity of IVDs in the normal group was the highest, whereas that in the other three groups showed obvious declines. The IVDs of UCMSC-exos-injected rats displayed significantly higher signal intensity than those of PBS-injected rats (Fig. 8A). H&E, Safranin O and Alcian blue staining were applied to evaluate the morphological changes of rat IVDs. Compared to the control group, severe atrophy of NPs and massive loss of proteoglycans occurred in the IVDD group. However, UCMSC-exos injection alleviated these histopathological changes in NP tissues, which were characterized by mild contraction of NPs and a slight loss of proteoglycans (Fig. 8B). Moreover, immunofluorescence staining results displayed that COL2A1 and TFAM expressions of NP section were remarkably decreased in the rat IVDD model, whereas UCMSC-exos injection restored their expression (Fig. 8C and D). These data suggest that UCMSC-exos delay the progression of IVDD in rats, which is consistent with the ex vivo results.

4. Discussion

Exosomes contain key bioactive components and play important roles in intercellular communication. The superior differentiation-inducing potential and easy collection of UCMSCs make them an effective source of exosomes. In this study, we found that UCMSC-exos effectively promoted the proliferation and ECM synthesis of NPCs. H_2O_2 destroyed the mitochondrial structure and up-regulated the ROS and mitochondrial superoxide levels in NPCs. However, UCMSC-exos exhibited a significant protective effect against H_2O_2-induced mitochondrial deterioration. Moreover, 4D-LFQ proteomic results suggested that UCMSC-exos increased the expression of mitochondrial protein TFAM to attenuate H_2O_2-induced mitochondrial dysfunction in NPCs.

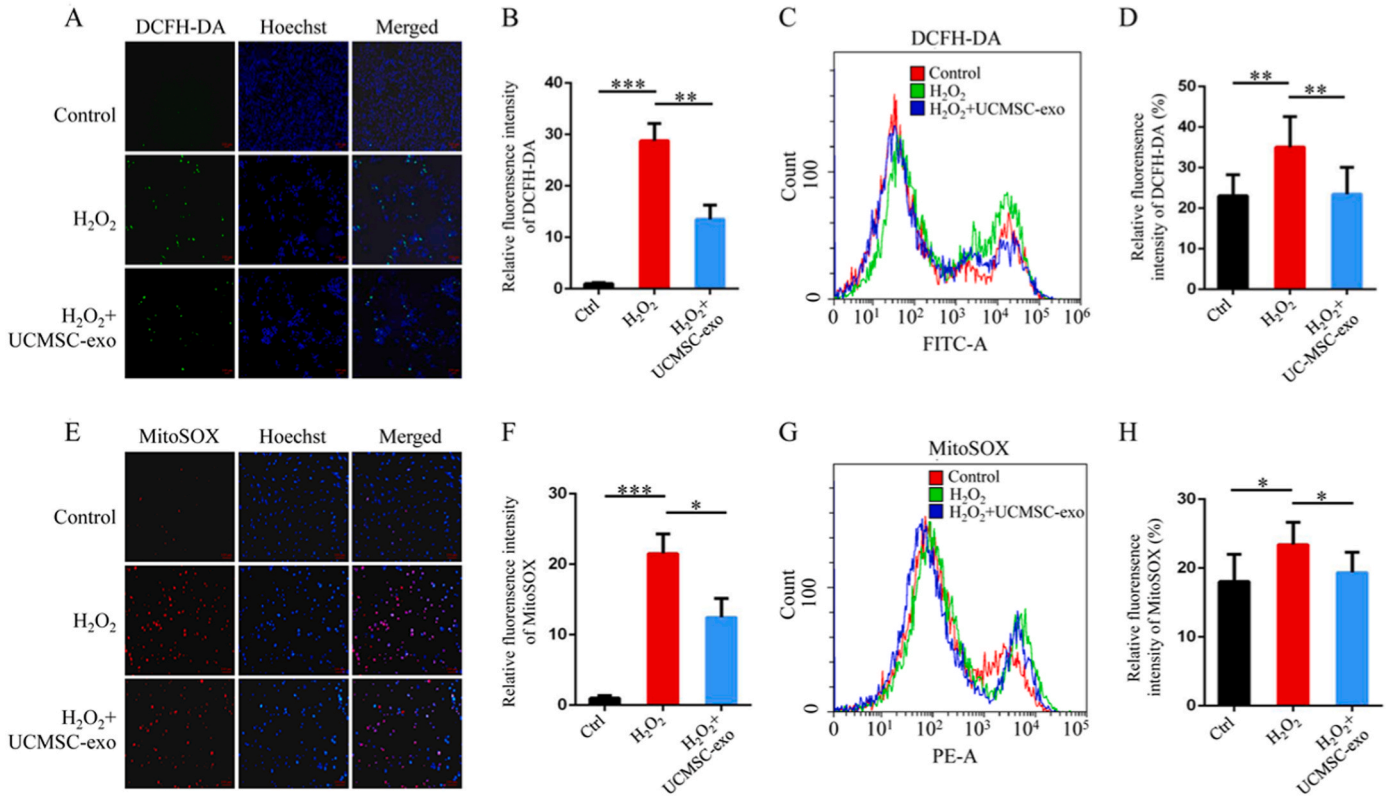

Figure 5. UCMSC-exos relieve H_2O_2-induced mitochondria oxidative stress of NPCs. (A) DCFH-DA (10 μM) was used to assess the cellular ROS level of H_2O_2-stimulated NPCs with UCMSC-exos treatment. The fluorescence intensity of DCFH-DA was observed by laser scanning confocal microscope. Scale bar: 100 μm. (B) Relative fluorescence intensity of DCFH-DA was quantified using Image J software. ***$P < 0.001$ H_2O_2 *vs* Ctrl group; **$P < 0.01$ H_2O_2+ UCMSC-exo *vs* H_2O_2 group. (C, D) Flow cytometry analysis of the fluorescence intensity of DCFH-DA. Data are presented as mean ± SD for three independent experiments, n = 3, **$P < 0.01$. (E) MitoSox Red (5 μM) was used to determine the mitochondrial ROS production in NPCs. The stained cells were imaged by laser scanning confocal microscope. Scale bar: 100 μm. (F) Relative fluorescence intensity of MitoSox Red was quantified using Image J software. ***$P < 0.001$ H_2O_2 *vs* Ctrl group; *$P < 0.05$ H_2O_2+ UCMSC-exo *vs* H_2O_2 group. (G, H) Flow cytometry analysis of the fluorescence intensity of MitoSox Red. Data are shown as mean ± SD for three independent experiments, n = 3, *$P < 0.05$. (For interpretation of the references to color in this figure legend, the reader is referred to the Web version of this article.)

High-throughput sequencing and qRT-PCR uncovered that UCMSC-exos down-regulated the levels of miR-194-5p, a potential negative regulator of TFAM, induced by H_2O_2. To clarify whether UCMSC-exos exerts such protective effects in vivo, we used a rat model of IVDD. Consistent with the ex vivo results, UCMSC-exos significantly delayed IVDD progression in rats.

IVD consists of three distinct but interdependent tissues including AF, NP and cartilage end-plates. IVDD is characterized by loss of NPCs, destruction of ECM, and accumulation of inflammatory cytokines. Degenerated NPCs proliferate at a reduced rate and undergo senescence, apoptosis or pyroptosis. Our results showed that UCMSC-exos markedly accelerated the proliferation of degenerated NPCs. Increased intracellular ROS levels induce the expression of matrix-degrading proteases [30]. In this study, we found that H_2O_2 promoted intracellular ROS production and ECM degradation in NPCs ex vivo, as confirmed by the up-regulation of MMP13 and down-regulation of ECM-related protein COL2A1. The addition of UCMSC-exos to H_2O_2-stimulated NPCs suppressed the up-regulation of ROS and MMP13 and the down-regulation of COL2A1. These results suggest that UCMSC-exos promote proliferation and repress ROS production and ECM degradation to physiologically restore the phenotype of degenerated NPCs.

Oxidative stress is closely associated with the pathogenesis of age-related diseases, including IVDD [21,22]. Chen et al. have reported that oxidative stress causes necroptosis and apoptosis of NPCs [31]. Several studies have shown that oxidative stress leads to mitochondrial dysfunction and increases ROS production. Disruption of mitochondrial structure and function has been observed in degenerated NPCs and IVDs [23,24]. In this study, we found that H_2O_2-induced oxidative stress damaged the mitochondrial cristae, resulting in abnormal mitochondria. Consequently, the dysfunctional mitochondria produced more ROS and superoxide, which causes DNA, protein damage and NPCs death. Recent studies have reported that BMSCs-exos alleviate compression-induced NPC apoptosis by inhibiting oxidative stress. Our data demonstrated that UCMSC-exos could relieve H_2O_2-induced oxidative stress in NPCs by restoring the normal mitochondrial structure and reducing ROS production. Excessive mitophagy induced by strong oxidative conditions promotes NPCs apoptosis [27]. PINK1/Parkin-dependent mitophagy, a selective form of autophagy involved in the degradation of damaged mitochondria, is critical for mitochondrial quality control. PINK1 accumulates on the mitochondrial surface and recruits the E3 ligase Parkin, leading to the ubiquitination of mitochondrial substrates, recruitment of autophagy receptors, and ultimately degradation of impaired mitochondria [32,33]. Our results showed that H_2O_2 stimulation significantly induced mitophagy in NPCs, accompanied by an increase in LC3-II/I ratio and PINK1 expression. After subsequent incubation with UCMSC-exos, we observed a decrease in LC3-II/I ratio, implying that UCMSC-exos attenuated mitophagy induced by H_2O_2 in NPCs. Interestingly, PINK1 expression was further augmented by UCMSC-exos. A previous study reported that hUCMSC-exos could transfer PINK1 mRNA to cardiomyocytes to increase PINK1 protein levels and prevent mitochondrial calcium overload in sepsis [34]. In NPCs, excessive ROS are critical activators of endoplasmic reticulum stress (ERS), leading to mitochondrial Ca^{2+} (mCa^{2+}) accumulation and subsequent necrosis [35]. Moreover, Ca^{2+} overload in mitochondria leads to the opening of mitochondrial permeability transition pore (MPTP) and depolarization of mitochondrial membrane potential

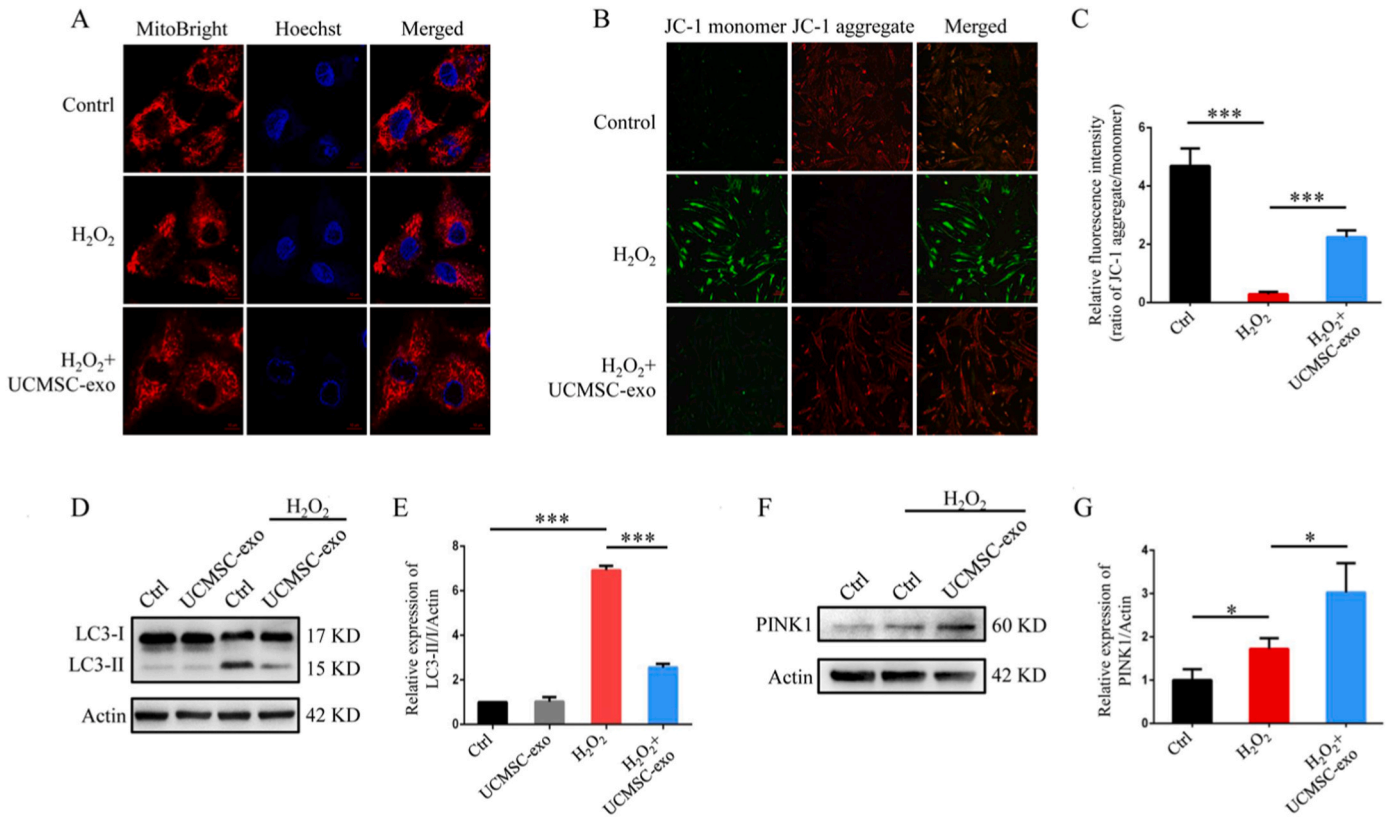

Figure 6. UCMSC-exos alleviate mitophagy and mitochondrial dysfunction in H_2O_2-stimulated NPCs. (A) The mitochondria of NPCs were stained by MitoBright LT Deep Red (0.1 μM) and observed by laser scanning confocal microscope. Cells were exposed to H_2O_2 and treated with UCMSC-exos. Scale bar: 10 μm. (B) JC-1 (10 μg/mL) was used to evaluate the MMP in NPCs. The fluorescence intensity of red JC-1 aggregate and green monomer was observed by laser scanning confocal microscope. Scale bar: 200 μm. (C) Ratio of red JC-1 aggregate/green monomer was quantified using Image J software. $^{***}P < 0.001$. (D, E) Western blot analysis of LC3 expression in NPCs. Relative protein expression level of LC3 was quantified using Image J software. $^{***}P < 0.001$. (F, G) Measurement of the PINK1 protein level in NPCs by western blot. Relative protein expression level of PINK1 was quantified using Image J software. $^{*}P < 0.05$. (For interpretation of the references to color in this figure legend, the reader is referred to the Web version of this article.)

(ΔΨm), which induces mitochondrial dysfunction and apoptosis [36]. It has been demonstrated that up-regulated PINK1 increases PKA activity to activate NCLX-mediated mCa^{2+} efflux and protect cardiomyocytes from injury [34]. Based on the inhibitory effect of UCMSC-exos on abnormal mitochondria and apoptosis, we speculate that UCMSC-exos may participate in the recovery of mitochondrial Ca^{2+} flux by up-regulating PINK1 in H_2O_2-induced NPCs. However, further research is required to validate these hypotheses.

To explore the molecular mechanism of UCMSC-exos, we analyzed the influence of UCMSC-exos on mitochondrial proteins in damaged NPCs. First, we identified DEPs between UCMSC-exos-treated and untreated H_2O_2-stimulated NPCs using 4D-LFQ proteomics. We then intersected the down-regulated proteins in H vs C with the up-regulated proteins in H_E vs H using a Venn diagram and identified the mitochondria-related protein TFAM. Consistent with the proteomic data, western blotting also showed that TFAM was significantly down-regulated by H_2O_2 but up-regulated by UCMSC-exos in NPCs ex vivo. Furthermore, immunofluorescence staining of rat IVDs displayed that UCMSC-exos injection could enhance TFAM expression in the rat IVDD model. TFAM is essential for the maintenance of mtDNA copy number and transcription initiation [37–39]. Loss of TFAM leads to mtDNA nucleoid instability, metabolic disorders, and cell death. TFAM-deficient mice exhibit mtDNA depletion, bioenergetic insufficiency, and embryonic lethality [40]. Here, for the first time, we revealed the role of TFAM in IVDD. In summary, our data demonstrate that UCMSC-exos can increase TFAM expression in NPCs under oxidative stress, thereby attenuating mtDNA damage and mitochondrial dysfunction.

This study highlights UCMSC-exos as promising nanotherapeutics for delaying the progression of IVDD. However, it has several limitations. Our data indicated that UCMSC-exos could relieve oxidative stress, attenuate mitochondrial dysfunction and inhibit apoptosis (Supplementary Fig. 2) in H_2O_2-induced NPCs. However, the effects of UCMSC-exos on H_2O_2-induced NPC inflammation remain unclear and require further investigation. Second, our data suggested that UCMSC-exos increased TFAM expression by inhibiting miR-194-5p in H_2O_2-induced NPCs. Nevertheless, the mechanism by which UCMSC-exos down-regulate H_2O_2-induced miR-194-5p expression remains unknown. Finally, due to the complexity and time-consuming nature of animal experiments, the expression of miR-194-5p has not been verified. In the future research, we will attempt to elucidate the regulatory mechanism of miR-194-5p by UCMSC-exos and the change of miR-194-5p expression in rat IDD model.

5. Conclusions

In conclusion, UCMSC-exos not only effectively promote ECM synthesis and proliferation of degenerated NPCs, but also relieve mitochondrial oxidative stress and attenuate mitochondrial dysfunction to maintain IVD homeostasis. Moreover, UCMSC-exos increase the mitochondrial protein TFAM expression by inhibiting miR-194-5p in H_2O_2-induced NPCs. These findings suggest UCMSC-exos as promising nanotherapeutics for IVDD.

Data availability

The data used to support the findings of this study are available from

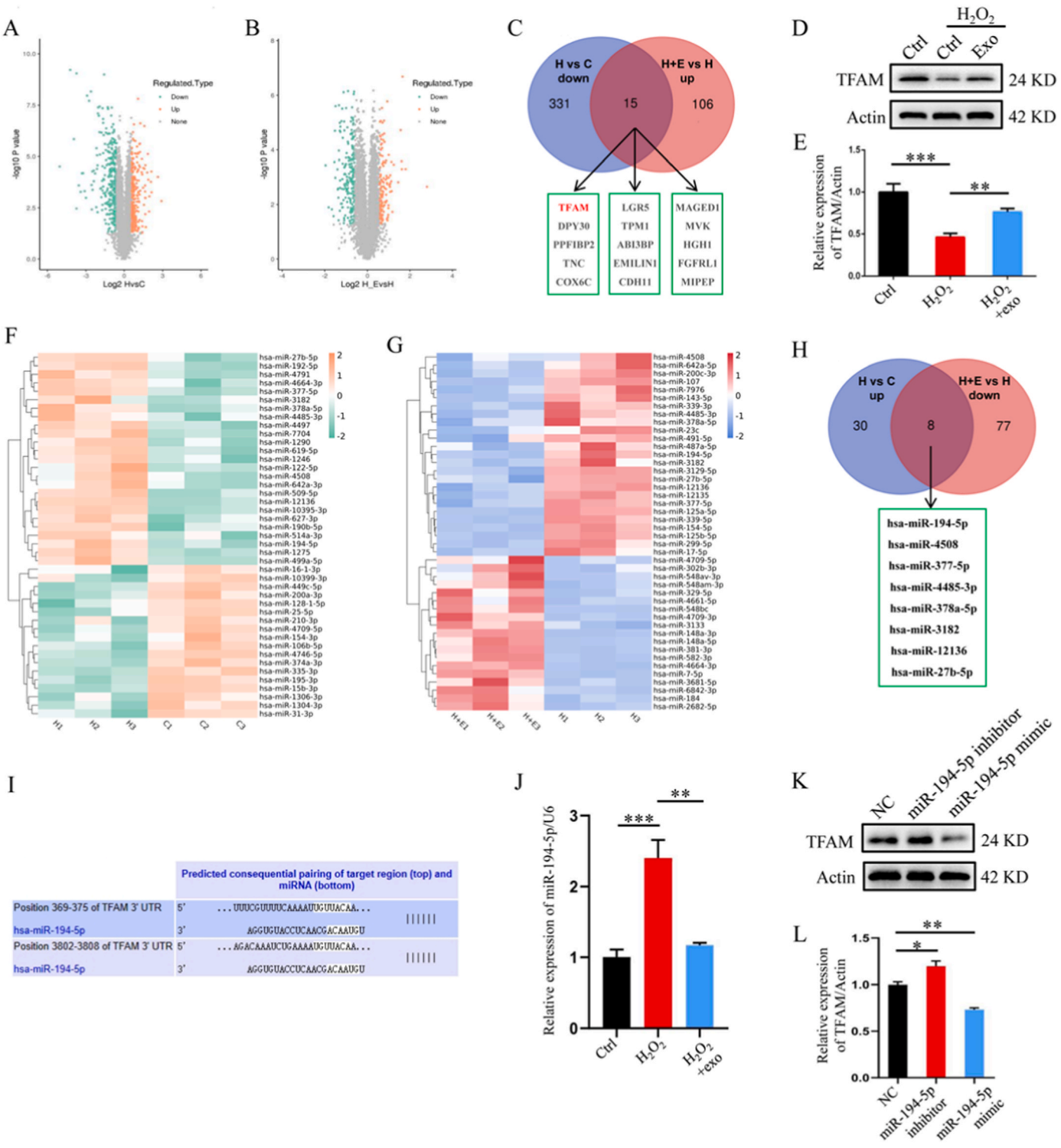

Figure 7. UCMSC-exos up-regulate mitochondrial protein TFAM and down-regulate miR-194-5p in H_2O_2-stimulated NPCs. (A, B) Volcano map of DEPs in the H *vs* C group (A) and H_E *vs* H (B) group. Orange dots represents up-regulated proteins, green dots shows down-regulated proteins, and grey dots means non-changed proteins. (C) Venn diagram displayed the shared proteins between the H *vs* C group and H_E *vs* H group. (D, E) Western blot analysis of TFAM expression in NPCs. Relative protein expression level of TFAM was quantified using Image J software. ***$P < 0.001$ H_2O_2 *vs* Ctrl group; **$P < 0.01$ H_2O_2+ UCMSC-exo *vs* H_2O_2 group. (F, G) Heat map of DE miRNAs in the H *vs* C group (F) and H + E *vs* H (G) group. (H) Venn diagram displayed the shared miRNAs between the H *vs* C group and H + E *vs* H group. (I) TargetScan database predicts the interaction sites between miR-194-5p and TFAM. (J) Quantitative analysis of miR-194-5p expression in NPCs by qRT-PCR. (K, L) Western blot analysis of TFAM expression in NPCs transfected with miR-194-5p inhibitors or mimics. Relative protein expression level of TFAM was quantified using Image J software. *$P < 0.05$ miR-194-5p inhibitor *vs* NC; **$P < 0.01$ miR-194-5p mimic *vs* NC. (For interpretation of the references to color in this figure legend, the reader is referred to the Web version of this article.)

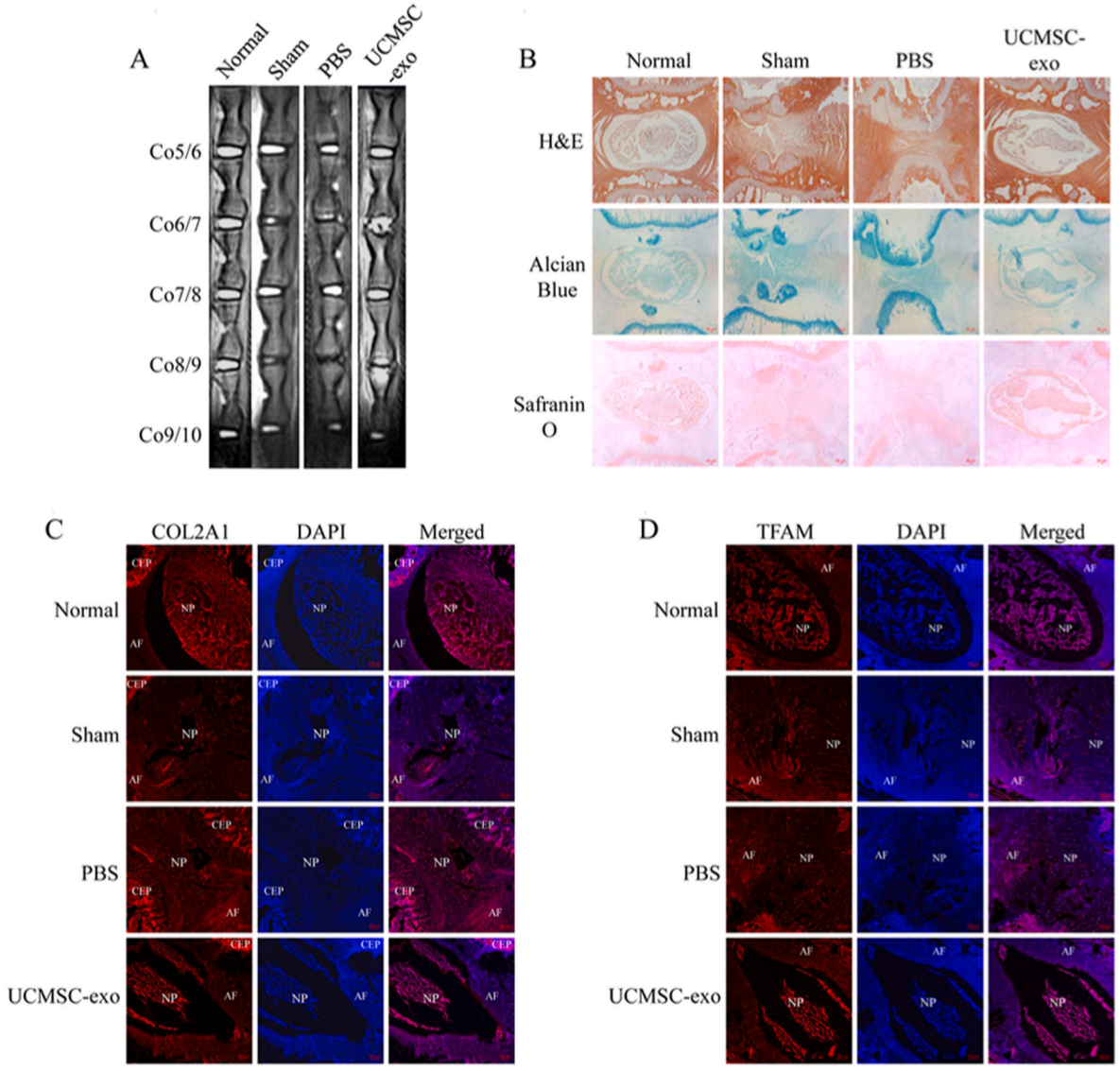

Figure 8. UCMSC-exos ameliorate the intervertebral disc degeneration in vivo. (A) T2-weighted MRIs of the rat tail discs were obtained at 8 weeks after needle puncture. Rats were divided into four groups: non-injured control group (normal), punctured group (sham), punctured with PBS treatment group (PBS), punctured with UCMSC-exos treatment group (UCMSC-exo). Co6/7 and Co8/9 were punctured with Co5/6, Co7/8 and Co9/10 left intact. (B) Hematoxylin and eosin (H&E), Safranin O and Alcian blue staining in the rat tail discs of Co6/7 or Co8/9 at 8 weeks after needle puncture. Scale bar: 20 μm. (C, D) IF staining of COL2A1 and TFAM in the rat tail discs of Co6/7 or Co8/9 at 8 weeks after needle puncture. Scale bar: 100 μm. (For interpretation of the references to color in this figure legend, the reader is referred to the Web version of this article.)

the corresponding author upon request.

Funding

This study was supported by the National Natural Science Foundation of China (Grant No. 81974345), Key Project of Natural Science Foundation of Shandong Province (Grant No. ZR2020KH010) and Youth Project of Natural Science Foundation of Shandong Province (Grant No. ZR2021QH059).

Declaration of competing interest

The authors declare that the research was conducted in the absence of any commercial or financial relationships that could be construed as a potential conflict of interest.

Acknowledgments

We would like to thank Hangzhou Jingjie Biotechnology Company for proteomic sequencing and data analysis.

Appendix A. Supplementary data

Supplementary data to this article can be found online at https://doi.org/10.1016/j.jot.2023.10.004.

References

[1] Francisco V, Pino J, Gonzalez-Gay MA, Lago F, Karppinen J, Tervonen O, et al. A new immunometabolic perspective of intervertebral disc degeneration. Nat Rev Rheumatol 2022;18(1):47–60.
[2] Khan AN, Jacobsen HE, Khan J, Filippi CG, Levine M, Lehman RA, et al. Inflammatory biomarkers of low back pain and disc degeneration: a review. Ann N Y Acad Sci 2017;1410(1):68–84.

[3] Cyg, Pc, Hhz. Roles of NLRP3 inflammasome in intervertebral disc degeneration. Osteoarthritis Cartilage 2021;29(6):793–801.
[4] Vergroesen PP, Kingma I, Emanuel KS, Hoogendoorn RJ, Welting TJ, van Royen BJ, et al. Mechanics and biology in intervertebral disc degeneration: a vicious circle. Osteoarthritis Cartilage 2015;23(7):1057–70.
[5] Cheng Z, Xiang Q, Wang J, Zhang Y. The potential role of melatonin in retarding intervertebral disc ageing and degeneration: a systematic review. Ageing Res Rev 2021;70:101394.
[6] Bailey CS, Rasoulinejad P, Taylor D, Sequeira K, Miller T, Watson J, et al. Surgery versus conservative care for persistent sciatica lasting 4 to 12 months. N Engl J Med 2020;382(12):1093–102.
[7] Richardson SM, Hughes N, Hunt JA, Freemont AJ, Hoyland JA. Human mesenchymal stem cell differentiation to NP-like cells in chitosan-glycerophosphate hydrogels. Biomaterials 2008;29(1):85–93.
[8] Vadala G, Ambrosio L, Russo F, Papalia R, Denaro V. Interaction between mesenchymal stem cells and intervertebral disc microenvironment: from cell therapy to tissue engineering. Stem Cell Int 2019;2019:2376172.
[9] Chen S, Zhao L, Deng X, Shi D, Wu F, Liang H, et al. Mesenchymal stem cells protect nucleus pulposus cells from compression-induced apoptosis by inhibiting the mitochondrial pathway. Stem Cell Int 2017;2017:9843120.
[10] Borem R, Madeline A, Bowman M, Gill S, Tokish J, Mercuri J. Differential effector response of amnion- and adipose-derived mesenchymal stem cells to inflammation; implications for intradiscal therapy. J Orthop Res 2019;37(11):2445–56.
[11] Li H, Liang C, Tao Y, Zhou X, Li F, Chen G, et al. Acidic pH conditions mimicking degenerative intervertebral discs impair the survival and biological behavior of human adipose-derived mesenchymal stem cells. Exp Biol Med 2012;237(7):845–52.
[12] Gilbert HTJ, Hodson N, Baird P, Richardson SM, Hoyland JA. Acidic pH promotes intervertebral disc degeneration: acid-sensing ion channel -3 as a potential therapeutic target. Sci Rep 2016;6:37360.
[13] Liang W, Han B, Hai Y, Sun D, Yin P. Mechanism of action of mesenchymal stem cell-derived exosomes in the intervertebral disc degeneration treatment and bone repair and regeneration. Front Cell Dev Biol 2021;9:833840.
[14] Bhujel B, Shin HE, Choi DJ, Han I. Mesenchymal stem cell-derived exosomes and intervertebral disc regeneration: review. Int J Mol Sci 2022;23(13).
[15] Rao D, Huang D, Sang C, Zhong T, Zhang Z, Tang Z. Advances in mesenchymal stem cell-derived exosomes as drug delivery vehicles. Front Bioeng Biotechnol 2021;9:797359.
[16] Tang Y, Zhou Y, Li HJ. Advances in mesenchymal stem cell exosomes: a review. Stem Cell Res Ther 2021;12(1):71.
[17] Cheng X, Zhang G, Zhang L, Hu Y, Zhang K, Sun X, et al. Mesenchymal stem cells deliver exogenous miR-21 via exosomes to inhibit nucleus pulposus cell apoptosis and reduce intervertebral disc degeneration. J Cell Mol Med 2018;22(1):261–76.
[18] Sun Y, Zhang W, Li X. Induced pluripotent stem cell-derived mesenchymal stem cells deliver exogenous miR-105-5p via small extracellular vesicles to rejuvenate senescent nucleus pulposus cells and attenuate intervertebral disc degeneration. Stem Cell Res Ther 2021;12(1):286.
[19] Yuan X, Li T, Shi L, Miao J, Guo Y, Chen Y. Human umbilical cord mesenchymal stem cells deliver exogenous miR-26a-5p via exosomes to inhibit nucleus pulposus cell pyroptosis through METTL14/NLRP3. Mol Med 2021;27(1):91.
[20] Xia C, Zeng Z, Fang B, Tao M, Gu C, Zheng L, et al. Mesenchymal stem cell-derived exosomes ameliorate intervertebral disc degeneration via anti-oxidant and anti-inflammatory effects. Free Radic Biol Med 2019;143:1–15.
[21] Feng C, Yang M, Lan M, Liu C, Zhang Y, Huang B, et al. ROS: crucial intermediators in the pathogenesis of intervertebral disc degeneration. Oxid Med Cell Longev 2017;2017:5601593.
[22] Yu H, Hou G, Cao J, Yin Y, Zhao Y, Cheng L. Mangiferin alleviates mitochondrial ROS in nucleus pulposus cells and protects against intervertebral disc degeneration via suppression of NF-kappaB signaling pathway. Oxid Med Cell Longev 2021;2021:6632786.
[23] Ma H, Xie C, Chen Z, He G, Dai Z, Cai H, et al. MFG-E8 alleviates intervertebral disc degeneration by suppressing pyroptosis and extracellular matrix degradation in nucleus pulposus cells via Nrf2/TXNIP/NLRP3 axis. Cell Death Dis 2022;8(1):209.
[24] Zhang Z, Wu J, Teng C, Wang J, Yu J, Jin C, et al. Orientin downregulating oxidative stress-mediated endoplasmic reticulum stress and mitochondrial dysfunction through AMPK/SIRT1 pathway in rat nucleus pulposus cells in vitro and attenuated intervertebral disc degeneration in vivo. Apoptosis 2022;27(11-12):1031-1048.
[25] Marycz K, Kornicka K, Szlapka-Kosarzewska J, Weiss C. Excessive endoplasmic reticulum stress correlates with impaired mitochondrial dynamics, mitophagy and apoptosis, in liver and adipose tissue, but not in muscles in EMS horses. Int J Mol Sci 2018;19(1).
[26] Su SH, Wu YF, Wang DP, Hai J. Inhibition of excessive autophagy and mitophagy mediates neuroprotective effects of URB597 against chronic cerebral hypoperfusion. Cell Death Dis 2018;9(7):733.
[27] Xu WN, Zheng HL, Yang RZ, Liu T, Yu W, Zheng XF, et al. Mitochondrial NDUFA4L2 attenuates the apoptosis of nucleus pulposus cells induced by oxidative stress via the inhibition of mitophagy. Exp Mol Med 2019;51(11):1–16.
[28] Hu Z, Wang Y, Gao X, Zhang Y, Liu C, Zhai Y, et al. Optineurin-mediated mitophagy as a potential therapeutic target for intervertebral disc degeneration. Front Pharmacol 2022;13:893307.
[29] Zhang H, La Marca F, Hollister SJ, Goldstein SA, Lin CY. Developing consistently reproducible intervertebral disc degeneration at rat caudal spine by using needle puncture. J Neurosurg Spine 2009;10(6):522–30.
[30] Tochhawng L, Deng S, Pugalenthi G, Kumar AP, Lim KH, Tan TZ, et al. Gelsolin-Cu/ZnSOD interaction alters intracellular reactive oxygen species levels to promote cancer cell invasion. Oncotarget 2016;7(33):52832–48.
[31] Chen S, Lv X, Hu B, Zhao L, Li S, Li Z, et al. Critical contribution of RIPK1 mediated mitochondrial dysfunction and oxidative stress to compression-induced rat nucleus pulposus cells necroptosis and apoptosis. Apoptosis 2018;23(5–6):299–313.
[32] Gladkova C, Maslen SL, Skehel JM, Komander D. Mechanism of parkin activation by PINK1. Nature 2018;559(7714):410–4.
[33] Gan ZY, Callegari S, Cobbold SA, Cotton TR, Mlodzianoski MJ, Schubert AF, et al. Activation mechanism of PINK1. Nature 2022;602(7896):328–35.
[34] Zhou Q, Xie M, Zhu J, Yi Q, Tan B, Li YS, et al. PINK1 contained in huMSC-derived exosomes prevents cardiomyocyte mitochondrial calcium overload in sepsis via recovery of mitochondrial Ca^{2+} efflux. Stem Cell Res Ther 2021;12(1):269.
[35] Lin H, Peng YZ, Li JY, Wang Z, Chen S, Qing XC, et al. Reactive oxygen species regulate endoplasmic reticulum stress and ER-mitochondrial Ca^{2+} crosstalk to promote programmed necrosis of rat nucleus pulposus cells under compression. 2021. Oxid Med Cell Longev 2021: 8810698.
[36] Xu HX, Cui SM, Zhang YM, Ren J. Mitochondrial Ca2+ regulation in the etiology of heart failure: physiological and pathophysiological implications. Acta Pharmacol Sin 2020;41(10):1301–9.
[37] Kang D, Kim SH, Hamasaki N. Mitochondrial transcription factor A (TFAM): roles in maintenance of mtDNA and cellular functions. Mitochondrion 2007;7(1–2):39–44.
[38] Picca A, Lezza AM. Regulation of mitochondrial biogenesis through TFAM-mitochondrial DNA interactions: useful insights from aging and calorie restriction studies. Mitochondrion 2015;25:67–75.
[39] Kunkel GH, Chaturvedi P, Tyagi SC. Mitochondrial pathways to cardiac recovery: TFAM. Heart Fail Rev 2016;21(5):499–517.
[40] Larsson NG, Wang J, Wilhelmsson H, Oldfors A, Rustin P, Lewandoski M, et al. Mitochondrial transcription factor A is necessary for mtDNA maintenance and embryogenesis in mice. Nat Genet 1998;18(3):231–6.